Bearings-Only Tracking with Fusion from Heterogenous Passive Sensors: ESM/EO and Acoustic

RONG YANG
YAAKOV BAR-SHALOM
GEE WAH NG

The performance of the conventional bearings-only tracking (BOT) from a single passive sensor hinges on the sensor platform maneuvers. This paper presents a new BOT approach based on fusion from two heterogenous bearings-only sensors residing on the same moving or stationary platform. The two sensors are an ESM/EO with negligible propagation delay and an acoustic sensor with significant propagation delay. The time difference between the reception times of the two sensors (corresponding to the same emission time) is the acoustic propagation delay. Since target range information is contained in the acoustic propagation delay (which is not known but can be estimated), the target state is shown to be completely observable even when the platform is stationary. The observability is studied in this paper via the Fisher information matrix (FIM).

Two estimators are developed. They are the maximum likelihood (ML) estimator for batch estimation and the out-of-sequence measurements fusion from acoustic and ESM/EO sensors (OOSM-AE) for recursive estimation. It shows that the ML estimator for batch estimation attains the Cramér-Rao lower bound (CRLB)—it is statistically efficient—except in cases with a small number of measurements and the target heading close to the bearing from the sensor platform. The OOSM-AE is developed to handle out-of-sequence measurements (OOSM) due to the acoustic propagation delay. It consists of an unscented Kalman filter (UKF) to handle the in-sequence ESM/EO measurements and an OOSM unscented Gauss-Helmert filter (OOSM-UGHF) to handle the out-of-sequence acoustic measurements. Simulation results are presented to demonstrate the performance of this new BOT approach.

Manuscript received April 19, 2015; revised November 30, 2015 and April 6, 2016; released for publication May 4, 2016.

Refereeing of this contribution was handled by Paolo Braca.

Authors' addresses: R. Yang and G. Wah Ng, DSO National Laboratories, 20 Science Park Drive, Singapore 118230 (E-mail: yrong@dso.org.sg; ngeewah@dso.org.sg); Y. Bar-Shalom, Department of ECE, University of Connecticut, Storrs, CT 06269, USA (E-mail: ybs@engr.uconn.edu).

Y. Bar-Shalom is supported by ARO Grant W911NF-10-1-0369 .

I. INTRODUCTION

The commonly used passive sensors, like acoustic sensors, electronic support measures (ESM) sensors and electro-optical (EO) sensors, measure target bearings only. This makes the target state estimation from range-absent measurements a challenging problem.

Several approaches for this problem have been developed in the last four decades. The most popular one is to deploy a passive sensor on a maneuvering platform, and the target state is estimated using bearings-only tracking (BOT) or bearings-only target motion analysis (BO-TMA) [16] [1]. This approach requires the sensor platform to maneuver, so the target state is observable [17] [11] [6]. Since these maneuvers can interfere with the sensor platform's own mission (for example: to reach its destination as early as possible), BOT from a nonmaneuvering platform has attracted attention recently. Results showed that the BOT problem is indeed observable from a nonmaneuvering platform when the target is performing particular maneuvers (two-leg with constant speed, or constant turn) [13] [7]. However, there is still a gap to transition these results to real applications, for the target can maneuver in a manner unbeknownst to the observer.

The BOT approach has been extended to the Doppler-bearing tracking (DBT) approach in [18] [10]. This approach tracks the target state and emitted frequencies from bearing and Doppler shifted frequency measurements and the state can be estimated even when the platform is not maneuvering. The difficulty faced in DBT is to identify the target Doppler shifted frequencies from a noisy environment, especially when the target emitted frequencies are varying.

Another approach is to locate targets through triangulation from multiple stationary or moving passive sensors located at different positions. This approach needs to remove triangulation "ghosts" in multi-target scenarios, and can be solved as an S-D assignment problem, where S is the number of sensors. A Lagrangian relaxation approach was suggested to solve this problem when $S \geq 3$ [19] [8]. By making use of Doppler frequencies, the number of sensors can be reduced to 2 ($S = 2$) [22].

In this paper, we propose a new bearings-only approach to fuse measurements from two heterogenous passive sensors deployed on the same platform which can be *either moving or stationary*. The two sensors are a passive ESM/EO sensor, designated as s_1 and a passive acoustic sensor, designated as s_2. Both sensors measure target bearings only. The ESM/EO sensor's detections have no propagation delay, whereas the acoustic sensor receives the target signals after significant propagation delays. The time difference between the reception times of the two sensors (corresponding to the same emission time) is the acoustic propagation delay, and the target range can then be inferred from the estimates of

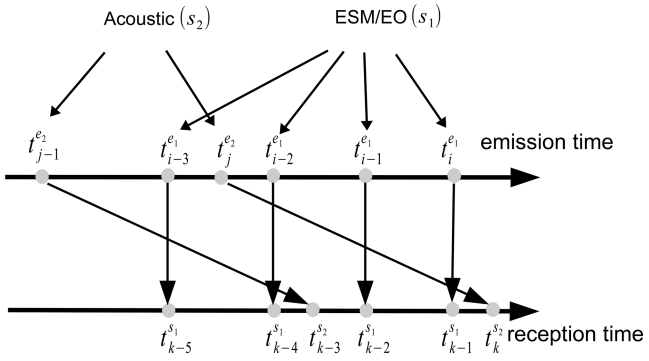

Fig. 1. Out-of-sequence measurements in ESM/EO and acoustic sensors.

these delays assuming the propagation speed is known. Complete observability in this BOT problem is therefore obtained, as range is implied in the sensors' reception times.

However, to obtain target range using the principle mentioned above is not straightforward. To compute the acoustic propagation delay, a pair of passive signals from s_1 and s_2 having the same emission time needs to be identified. A BOT target usually emits continuous signals which are received by the sensors and discretized by sampling. They are not instantaneous signals, like "ping" or "pulse" which can be associated easily. There is no feature to identify an acoustic bearing measurement and an ESM/EO measurement emitted at the same time. Furthermore, the ESM/EO and acoustic sensor may have different sampling times (they are asynchronous), and the sensor platform may be dynamic. These make the problem even more complicated.

Fig. 1 illustrates the ESM/EO and acoustic signal emission and reception time sequences, where k is the reception time index, which orders the combined acoustic and EO/ESM discretized signals by arrival (sensor) time. This is also the measurement index, while i and j are the target signal emission time indexes from s_1 and s_2, respectively. It can be seen that measurements arrive the observer out-of-sequence due to the acoustic propagation delay.

Our preliminary study on this problem has been presented in [25] recently. At the same time, the problem has also been addressed in [14]. In the present paper, we will conduct a comprehensive study, which includes the problem observability, appropriate algorithms from batch and recursive estimation and analyzing the efficiency of these estimators.

The structure of the rest of paper is as follows. Section II formulates the problem as a batch estimation problem, and develops a maximum likelihood (ML) estimator for the problem. Section III analyzes the observability of the problem via the Fisher Information Matrix (FIM). Section IV presents simulation results for the batch estimation and studies the estimator efficiency. Sections V–VII focus on the recursive estimation. Sections V and VI develop a novel recursive state estimation algorithm, and Section VII presents simulation results and recursive estimator efficiency analysis. Conclusions are given in Section VIII.

II. PROBLEM FORMULATION AND ML ESTIMATOR FOR THE BATCH ESTIMATION

This section formulates the acoustic and ESM/EO bearing fusion problem (designated as "AE") as a parameter estimation problem from a batch of bearing measurements. Since the BOT problem has been well studied when the platform is maneuvering, we focus on the stationary platform here. The target motion parameter $\mathbf{x}$ is to be estimated from the measurement vector $\mathbf{Z}$ consisting of a batch of ESM/EO (s_1) and acoustic (s_2) bearings. This is modeled as

$$\mathbf{Z} = \mathbf{h}(\mathbf{x}) + \mathbf{w} \tag{1}$$

where $\mathbf{h}(\cdot)$ is the function that relates $\mathbf{x}$ to $\mathbf{Z}$, and $\mathbf{w}$ is the measurement noise. The measurement vector $\mathbf{Z}$ is

$$\mathbf{Z} = [b(t_1^s)\cdots b(t_n^s)]' \tag{2}$$

where $s \in \{s_1, s_2\}$ is the sensor receiving the signal at time t_k^s. The parameter $\mathbf{x}$ consists of the position and velocity of the target at time t_n^s

$$\mathbf{x} = [x \;\; y \;\; \dot{x} \;\; \dot{y}]' \tag{3}$$

Assuming the measurement noises of s_1 and s_2 are zero-mean white Gaussian with the same standard deviation[1] σ_b, the covariance of $\mathbf{w}$ is

$$\mathbf{R} = \sigma_b^2 \mathbf{I}_n \tag{4}$$

where $\mathbf{I}_n$ is the identity matrix of dimension n.

The function that relates $\mathbf{x}$ to $\mathbf{Z}$ is

$$\mathbf{h}[\mathbf{x}] = [h(t_1^s, \mathbf{x})\cdots h(t_n^s, \mathbf{x})]' \tag{5}$$

where $h(\cdot)$ is the function that maps $\mathbf{x}$ to s_1 or s_2 bearings. Assuming the stationary sensor is located at (0,0), $h(\cdot)$ is given by

$$h(t_k^s, \mathbf{x}) = \begin{cases} \tan^{-1}\left[\dfrac{x-(t_n^s-t_k^s)\dot{x}}{y-(t_n^s-t_k^s)\dot{y}}\right] & \text{if } s = s_1 \\ \tan^{-1}\left[\dfrac{x-(t_n^s-t_k^s+\delta_{j,k})\dot{x}}{y-(t_n^s-t_k^s+\delta_{j,k})\dot{y}}\right] & \text{if } s = s_2 \end{cases} \tag{6}$$

where $\delta_{j,k}$ is the propagation delay of the jth acoustic bearing with arrival time t_k^s (see (44)–(45) and Fig. 1), which follows from the quadratic equation

$$[x-(t_n^s-t_k^s+\delta_{j,k})\dot{x}]^2 + [y-(t_n^s-t_k^s+\delta_{j,k})\dot{y}]^2 = (c^{\mathrm{p}}\delta_{j,k})^2 \tag{7}$$

[1]This is for simplicity of notation only.

The solution of the above is[2]

$$\delta_{j,k} = \frac{x_k^d \dot{x} + y_k^d \dot{y} \pm \phi_k}{\rho} = \frac{x_k^d \dot{x} + y_k^d \dot{y} - \phi_k}{\rho} \tag{8}$$

where

$$\phi_k = \sqrt{(x_k^d \dot{x} + y_k^d \dot{y})^2 - [(x_k^d)^2 + (y_k^d)^2]\rho} \tag{9}$$

$$\rho = \dot{x}^2 + \dot{y}^2 - (c^{\mathrm{p}})^2 \tag{10}$$

$$x_k^d = x - (t_n^s - t_k^s)\dot{x} \tag{11}$$

$$y_k^d = y - (t_n^s - t_k^s)\dot{y} \tag{12}$$

The ML estimate $\hat{\mathbf{x}}$ of $\mathbf{x}$ is obtained from the likelihood function $\Lambda(\mathbf{x};\mathbf{Z})$ of $\mathbf{x}$ based on the batch of measurements $\mathbf{Z}$ as

$$\hat{\mathbf{x}} = \arg\max_{\mathbf{x}} \Lambda(\mathbf{x};\mathbf{Z}) = \arg\max_{\mathbf{x}} p(\mathbf{Z} \mid \mathbf{x}) \tag{13}$$

Under the zero-mean Gaussian assumption on the noise $\mathbf{w}$, the above becomes the following nonlinear least squares (NLS) problem [2]

$$\hat{\mathbf{x}} = \arg\min_{\mathbf{x}} \{[\mathbf{Z} - \mathbf{h}(\mathbf{x})]' \mathbf{R}^{-1} [\mathbf{Z} - \mathbf{h}(\mathbf{x})]\} \tag{14}$$

which will be solved numerically via the iterated squares (ILS) method. The ILS yields the ML estimate of the parameter $\mathbf{x}(n)$ (at the end of the batch of length n) is as follows

$$\mathbf{P}^l = [\mathbf{H}[\hat{\mathbf{x}}^l(n)]' \mathbf{R}^{-1} \mathbf{H}[\hat{\mathbf{x}}^l(n)]]^{-1} \tag{15}$$

$$\hat{\mathbf{x}}^{l+1}(n) = \hat{\mathbf{x}}^l(n) + \mathbf{P}^l \mathbf{H}[\hat{\mathbf{x}}^l(n)]' \mathbf{R}^{-1} [\mathbf{Z} - \mathbf{h}[\hat{\mathbf{x}}^l(n)]] \tag{16}$$

where l is the iteration number, and $\mathbf{H} = (\cdot)$ the Jacobian matrix of $\mathbf{h}(\cdot)$. This is derived next.

$$\mathbf{H}(\mathbf{x}) = (\nabla_{\mathbf{x}} \mathbf{h}[\mathbf{x}]')' = [\mathbf{H}_1^s \cdots \mathbf{H}_n^s]' \tag{17}$$

where

$$\mathbf{H}_k^s = \begin{cases} \left[\dfrac{y_k^d}{(r_k^d)^2} \quad -\dfrac{x_k^d}{(r_k^d)^2} \quad -\dfrac{(t_n^s - t_k^s) y_k^d}{(r_k^d)^2} \quad \dfrac{(t_n^s - t_k^s) x_k^d}{(r_k^d)^2}\right]' \\ \text{if } s = s_1 \\ [H_{k,1}^s \;\; H_{k,2}^s \;\; H_{k,3}^s \;\; H_{k,4}^s]' \\ \text{if } s = s_2 \end{cases} \tag{18}$$

and (recall that j denotes the index of the acoustic bearing that arrives at t_k)

$$H_{k,1}^s = \frac{y_{j,k}^e + (x_{j,k}^e \dot{y} - y_{j,k}^e \dot{x}) \nabla_x \delta_{j,k}}{(r_{j,k}^e)^2} \tag{19}$$

$$H_{k,2}^s = \frac{-x_{j,k}^e + (x_{j,k}^e \dot{y} - y_{j,k}^e \dot{x}) \nabla_y \delta_{j,k}}{(r_{j,k}^e)^2} \tag{20}$$

$$H_{k,3}^s = \frac{-(t_n^s - t_k^s + \delta_{j,k}) y_{j,k}^e + (x_{j,k}^e \dot{y} - y_{j,k}^e \dot{x}) \nabla_{\dot{x}} \delta_{j,k}}{(r_{j,k}^e)^2} \tag{21}$$

$$H_{k,4}^s = \frac{(t_n^s - t_k^s + \delta_{j,k}) x_{j,k}^e + (x_{j,k}^e \dot{y} - y_{j,k}^e \dot{x}) \nabla_{\dot{y}} \delta_{j,k}}{(r_{j,k}^e)^2} \tag{22}$$

$$\nabla_x \delta_{j,k} = \frac{1}{\rho}\left[\dot{x} - \frac{(c^{\mathrm{p}})^2 x_k^d - \dot{y}(x_k^d \dot{y} - y_k^d \dot{x})}{\phi_k}\right] \tag{23}$$

$$\nabla_y \delta_{j,k} = \frac{1}{\rho}\left[\dot{y} - \frac{(c^{\mathrm{p}})^2 y_k^d + \dot{x}(x_k^d \dot{y} - y_k^d \dot{x})}{\phi_k}\right] \tag{24}$$

$$\begin{aligned} \nabla_{\dot{x}} \delta_{j,k} = \frac{1}{\rho}\Bigg[& x_k^d - (t_n^s - t_k^s)\dot{x} + \frac{(c^{\mathrm{p}})^2 (t_n^s - t_k^s) x_k^d}{\phi_k} \\ & - \frac{(x_k^d \dot{y} - y_k^d \dot{x})(y_k^d + (t_n^s - t_k^s)\dot{y})}{\phi_k}\Bigg] \\ & - \frac{2\dot{x}(x_k^d \dot{x} + y_k^d \dot{y} - \phi_k)}{\rho^2} \end{aligned} \tag{25}$$

$$\begin{aligned} \nabla_{\dot{y}} \delta_{j,k} = \frac{1}{\rho}\Bigg[& x_k^d - (t_n^s - t_k^s)\dot{x} + \frac{(c^{\mathrm{p}})^2 (t_n^s - t_k^s) y_k^d}{\phi_k} \\ & + \frac{(x_k^d \dot{y} - y_k^d \dot{x})(x_k^d + (t_n^s - t_k^s)\dot{x})}{\phi_k}\Bigg] \\ & - \frac{2\dot{y}(x_k^d \dot{x} + y_k^d \dot{y} - \phi_k)}{\rho^2} \end{aligned} \tag{26}$$

$$r_k^d = \sqrt{(x_k^d)^2 + (y_k^d)^2} \tag{27}$$

$$x_{j,k}^e = x - (t_n^s - t_k^s + \delta_{j,k})\dot{x} \tag{28}$$

$$y_{j,k}^e = y - (t_n^s - t_k^s + \delta_{j,k})\dot{y} \tag{29}$$

$$r_{j,k}^e = \sqrt{(x_{j,k}^e)^2 + (y_{j,k}^e)^2} \tag{30}$$

III. OBSERVABILITY ANALYSIS VIA THE FISHER INFORMATION MATRIX

To analyze the observability of the nonlinear model (1), the Fisher information matrix (FIM) will be used. The relationship between the FIM and parameter observability (i.e., its estimability) has been studied in [12]. The parameter $\mathbf{x}$ in (1) is completely observable, if the FIM is nonsingular (invertible). The FIM is given by [2]

$$\mathcal{F}(\mathbf{x}) = \mathbf{H}'(\mathbf{x}) \mathbf{R}^{-1} \mathbf{H}(\mathbf{x}) \tag{31}$$

where H is the Jacobian matrix given in (17).

[2]The negative sign is selected in (8.) so that the propagation delay $\delta_{j,k}$ is greater than 0, to match (6)–(7).

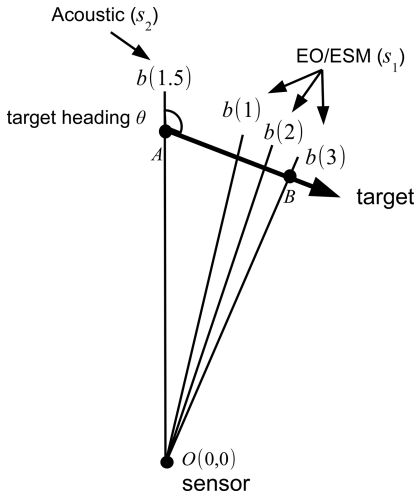

Fig. 2. Observability analysis. Estimation of the target position and velocity at point B using four bearings (the acoustic bearing's reception time is $t_2^{s_2}$ = 1.5s).

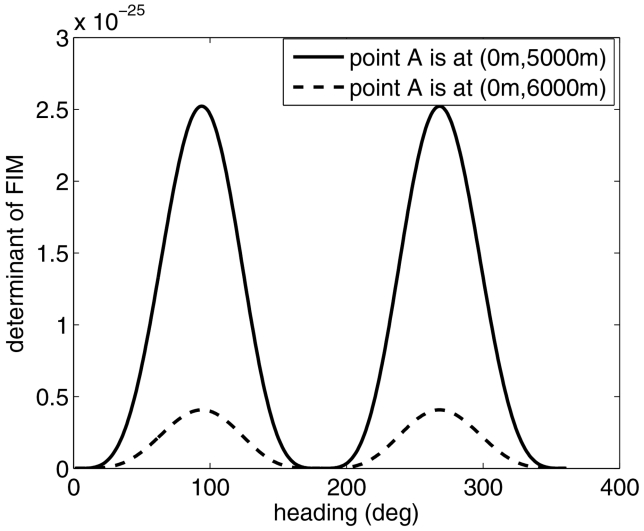

Fig. 3. det[$\mathcal{F}$] versus target heading when the target speed is 5 m/s.

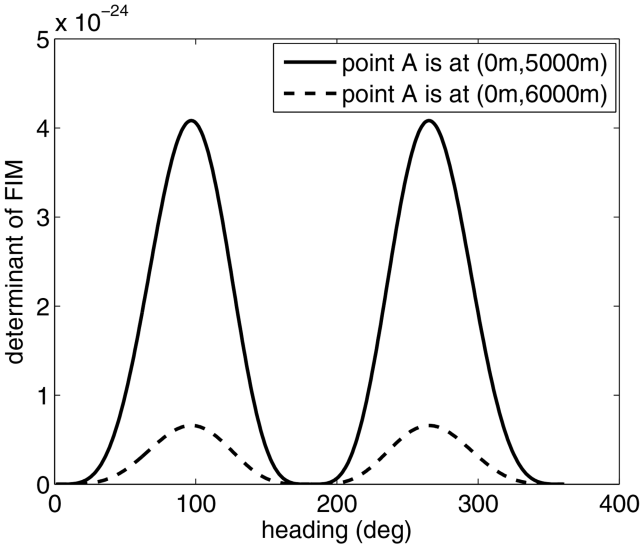

Fig. 4. det[$\mathcal{F}$] versus target heading when the target speed is 10 m/s.

Since the size of the parameter $\mathbf{x}$ is four, $\mathbf{Z}$ should consist of at least four bearings for observability. Fig. 2 illustrates the problem with three ESM/EO bearings received at times 1 s, 2 s and 3 s, and a delayed acoustic bearing with reception time 1.5 s, and

$$\mathbf{Z} = [b(1)\ \ b(1.5)\ \ b(2)\ \ b(3)]' \tag{32}$$

The parameter to be estimated is $\mathbf{x}$ at time t_4^s = 3s, which corresponds to point B on the trajectory $\overline{AB}$.

The observability analysis is based on the numerical results of det[$\mathcal{F}(\mathbf{x})$] for various geometries of the target trajectory and platform. The scenarios consist of the target trajectory $\overline{AB}$ rotating 360° around point A in Fig. 2, namely the target heading varies from 1° to 360°. The bearing error standard deviation for both sensors is $\sigma_b = 1°$ in the FIM. Figs. 3–6 show det[$\mathcal{F}(\mathbf{x})$] versus target heading with the target speeds of 5 m/s, 10 m/s, 50 m/s and 100 m/s respectively. In each figure, det[$\mathcal{F}(\mathbf{x})$] is investigated at two different ranges, namely, target motion starting point A is at (0 m, 5000 m) and (0 m, 6000 m).

From the results, we observe that FIM is singular (or det[$\mathcal{F}$] = 0) only when the target heading is at 180° and 360° w.r.t. the line-of-sight (LOS) to the sensor platform. The problem is unobservable in these cases, and the four bearings are the same and always in line with the target heading. Thus, we can conclude that the problem is completely observable unless the bearing is constant over time.

The FIM itself is the total information about the parameter $\mathbf{x}$ from the measurement set $\mathbf{Z}$. A higher value of det[$\mathcal{F}$] represents a better estimation of $\mathbf{x}$ from $\mathbf{Z}$. Obviously, the determinant of $\mathcal{F}$ is affected by the target range, speed and heading. It can be seen that the value of det[$\mathcal{F}$] is increasing with target speed and decreasing with target range. For the target heading, it closely links to the change of the bearings in the batch. Intuitively, a larger bearing change gives a better estimate. We can see that det[$\mathcal{F}$] almost reaches zero when the heading is close to 180° or 360°, where the bearing change is small. When the heading is away from 180° and 360°, det[$\mathcal{F}$] increases as the bearing change increases. However, the maximum det[$\mathcal{F}$] is not exactly on the target trajectory with the largest change in bearing. Target range is also taken into consideration in FIM. Fig. 7 shows that the trajectory $\overline{AB'}$ has the largest change in bearing. However it does not have the highest det[$\mathcal{F}$]. The trajectories with the highest det[$\mathcal{F}$] is $\overline{AB}$. This is because B is closer to the sensor than B'.

IV. SIMULATION RESULTS FOR THE BATCH ESTIMATION

The scenarios in the simulation are similar to those used in Section III but with different batch size. Point A in Fig. 7 is set at (0 m, 5000 m). The target speed is 100 m/s, and the heading is chosen from 10°–140°.

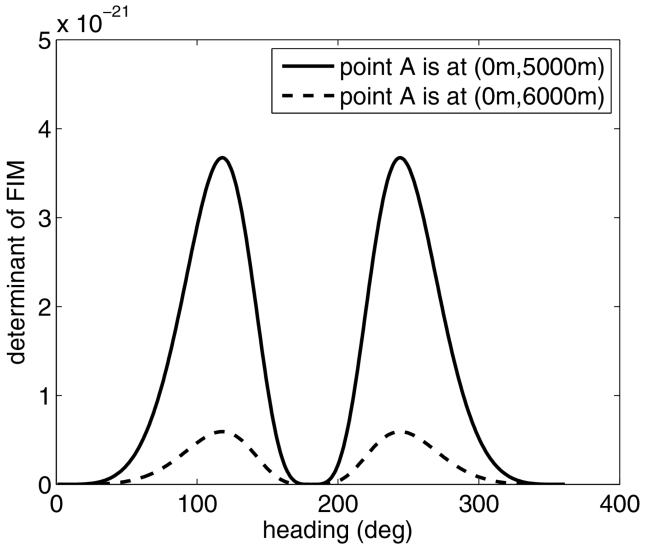

Fig. 5. det[$\mathcal{F}$] versus target heading when the target speed is 50 m/s.

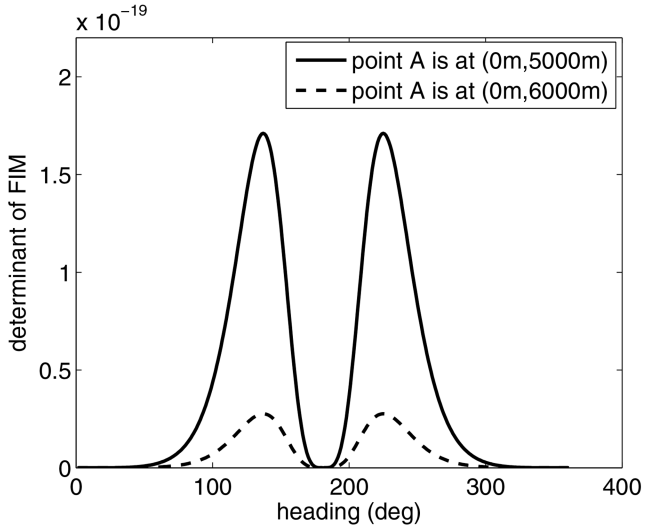

Fig. 6. det[$\mathcal{F}$] versus target heading when the target speed is 100 m/s.

The bearing error standard deviations for both s_1 and s_2 are set to $\sigma_b = 1^\circ$. Four different batch sizes are investigated, namely

- $n = 10$: 10 ESM/EO bearings and 5 acoustic bearings over a total time of 10 s.
- $n = 20$: 20 ESM/EO bearings and 10 acoustic bearings over a total time of 20 s.
- $n = 30$: 30 ESM/EO bearings and 15 acoustic bearings over a total time of 30 s.
- $n = 60$: 60 ESM/EO bearings and 30 acoustic bearings over a total time of 60 s.

This section also studies the CRLB of the problem, and compares the errors of the ILS estimates to the CRLB. The CRLB error covariance matrix $\mathbf{P}^{\text{CRLB}}$, which is a 4×4 matrix, is given by

$$\mathbf{P}^{\text{CRLB}} = \mathcal{F}^{-1} \tag{33}$$

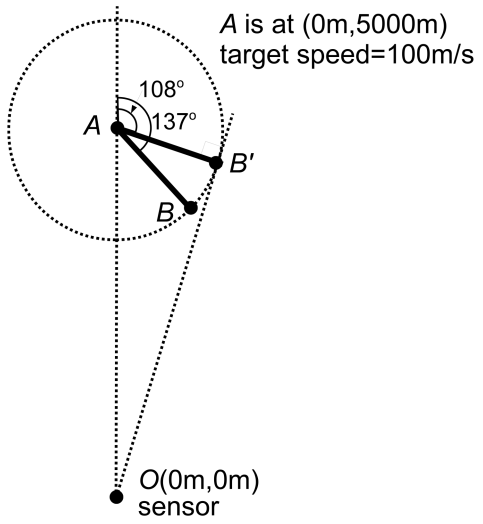

Fig. 7. The target trajectory $\overline{AB}$ has the highest det[$\mathcal{F}$], and $\overline{AB'}$ has the largest bearing change.

The CRLB-based root mean square errors (RMSE) of the position and velocity are

$$\text{pos}_{\text{batch}}^{\text{CRLB}} = \sqrt{\mathbf{P}_{11}^{\text{CRLB}} + \mathbf{P}_{22}^{\text{CRLB}}} \tag{34}$$

$$\text{vel}_{\text{batch}}^{\text{CRLB}} = \sqrt{\mathbf{P}_{33}^{\text{CRLB}} + \mathbf{P}_{44}^{\text{CRLB}}} \tag{35}$$

The ILS RMSEs of the final position and velocity estimates are computed based on 200 Monte Carlo runs for each of the above batches. They are given by

$$\text{pos}_{\text{batch}}^{\text{RMSE}} = \sqrt{\frac{1}{N}\sum_{i=1}^{N}[\text{pos}_{\text{batch},i}^{\text{err}}]^2} \tag{36}$$

$$\text{vel}_{\text{batch}}^{\text{RMSE}} = \sqrt{\frac{1}{N}\sum_{i=1}^{N}[\text{vel}_{\text{batch},i}^{\text{err}}]^2} \tag{37}$$

where i is the run index, $N = 200$ is the number of runs, and

$$\text{pos}_{\text{batch},i}^{\text{err}} = \sqrt{[\hat{x} - x]^2 + [\hat{y} - y]^2} \tag{38}$$

$$\text{vel}_{\text{batch},i}^{\text{err}} = \sqrt{[\hat{\dot{x}} - \dot{x}]^2 + [\hat{\dot{y}} - \dot{y}]^2} \tag{39}$$

where $\hat{x}$, $\hat{y}$, $\hat{\dot{x}}$ and $\hat{\dot{y}}$ are the estimated target position and velocity in x and y coordinates, respectively, x, y, $\dot{x}$ and $\dot{y}$ are the true target positions and velocities, respectively.

To evaluate the consistency of the estimates obtained via the ILS with the CRLB (i.e. its statistical efficiency), the normalized estimation error squared (NEES) [2] is evaluated. The full state NEES for N Monte Carlo runs is

$$\bar{\epsilon} = \frac{1}{N}\sum_{i=1}^{N}(\hat{\mathbf{x}}_i - \mathbf{x})'\mathcal{F}(\hat{\mathbf{x}}_i - \mathbf{x}) \tag{40}$$

where i is the run index.

Table I presents the ILS RMSEs of the position and velocity estimates versus the CRLBs. Fig. 8 shows

TABLE I
Estimate RMSEs versus CRLB

Batch size	Target heading (°)	Position CRLB (m)	Position ILS RMSE (m)	Velocity CRLB (m/s)	Velocity ILS RMSE (m/s)	NEES
	45	1961.0	2893.9	139.7	187.3	5.04
	50	1735.2	1962.3	124.4	130.3	4.17
	55	1548.3	1848.4	111.8	123.9	4.13
$n = 10$	60	1390.9	1498.2	101.2	107.6	4.23
	80	949.1	1020.4	72.0	77.5	4.01
	100	682.6	722.52	54.9	45.2	4.09
	120	502.6	535.1	45.3	46.9	4.31
	140	451.1	478.2	43.3	44.5	3.70
	20	2516.9	2680.5	118.1	122.8	4.60
	25	1994.3	2001.3	93.8	90.0	4.19
	30	1642.5	1653.3	77.5	77.5	4.28
	40	1195.5	1223.1	56.9	56.9	4.29
$n = 20$	60	731.3	753.7	35.6	37.2	4.24
	80	486.0	487.7	24.6	24.7	3.96
	100	333.5	343.9	17.8	18.3	3.81
	120	232.9	234.5	13.4	13.9	4.02
	140	169.9	174.2	10.9	11.4	4.06
	15	2565.2	3011.2	87.0	95.0	4.79
	20	1908.5	1970.0	64.8	64.8	4.02
	25	1511.0	1553.3	51.4	52.2	4.26
	40	902.5	915.8	31.0	31.8	4.23
$n = 30$	60	547.3	565.8	19.2	20.1	3.79
	80	358.2	361.9	12.9	13.2	4.20
	100	238.9	248.9	9.0	9.2	4.39
	120	157.7	160.6	6.4	6.5	3.70
	140	101.0	103.3	4.6	4.7	4.20
	10	2893.1	3066.2	48.4	62.6	4.50
	15	1917.7	2102.4	32.1	33.5	4.24
	20	1426.8	1452.1	23.9	24.8	4.25
	40	675.0	687.9	11.3	11.5	3.98
$n = 60$	60	409.8	433.6	6.9	7.2	4.05
	80	268.8	269.9	4.6	4.5	3.86
	100	180.3	182.2	3.2	3.2	3.71
	120	120.6	121.3	2.3	2.3	4.17
	140	80.0	81.5	1.8	1.8	3.75

the ILS RMSEs of position estimates versus CRLBs in graph form, where n in legends ILS-n and CRLB-n stands for the batch size. It can be seen that the estimates are very close to their CRLBs, except for the cases with marginal observability (e.g., $n = 10$ and heading $\theta = 45°$). In these cases the errors are large, and the ILS does not yield a statistically efficient estimate. Upon examining the reason why the estimate in these cases had large errors compared to the CRLB, it was observed that the likelihood $\Lambda(\mathbf{x};\mathbf{Z})$ is larger at the (bad) estimate than at the true value (i.e., better goodness of fit to the noisy data for the bad estimate). This is because of the noisiness of the likelihood function due to the combined effect of the small number of measurements and the marginal observability.

The NEES is also shown in Table I. The 95% of probability region upper limit for a 800 degrees of freedom ($N = 200$, the size of $\mathbf{x}$ is 4) chi-square random

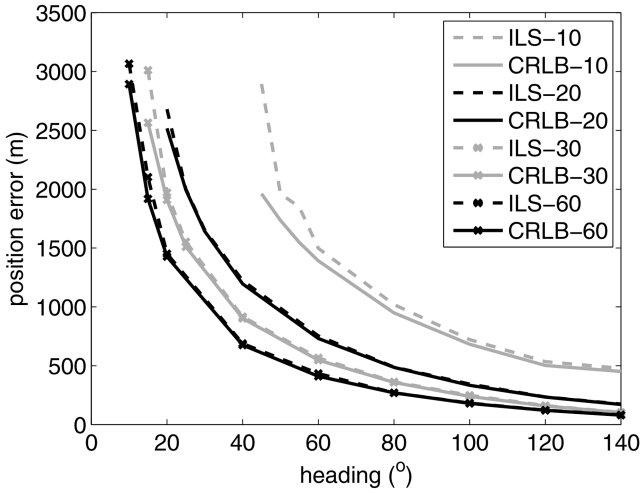

Fig. 8. Comparison of the ILS position estimation RMSE with the CRLB for $n = 10$, 20, 30 and 60.

variable is 867. Dividing by $N = 200$, the NEES $\bar{\epsilon}$ should be less than 4.33. We carry out a test between the hypotheses

$$\mathrm{H}_0: \quad \mathcal{P} = \mathbf{P}^{\mathrm{CRLB}} = \mathcal{F}^{-1} \tag{41}$$

$$\mathrm{H}_1: \quad \mathcal{P} > \mathbf{P}^{\mathrm{CRLB}} = \mathcal{F}^{-1} \tag{42}$$

where $\mathcal{P}$ is the actual covariance of the ML estimator. With the 95% probability region of $p(\bar{\epsilon} \mid \mathrm{H}_0)$ the test accepts H_0, i.e., it rejects H_1 at 5% significance level if

$$\bar{\epsilon} < 4.33 \tag{43}$$

In Table I, only 4 cases of the 35 cases considered do not satisfy (43). This shows that the ML estimate obtained via ILS yields results consistent with the CRLB in most of the cases. The four inconsistent cases (the first case in each batch category) are inserted on purpose, so that one can find the estimator's limitation through the NEES. We reduced the heading θ in each batch category until the NEES exceeds 4.33. It can be seen that the NEES exceeded 4.33 at $\theta = 45°$ when $n = 10$, whereas this occurs at $\theta = 10°$ when $n = 60$. Thus, the region of the ILS where the performance is consistent with the CRLB increases with the batch size.

Therefore the estimator's actual covariance is equal to the CRLB (with the exceptions noted above), i.e., the estimator presented is *statistically efficient*. This is in accordance to the well known property of the ML estimator that it is asymptotically efficient, i.e., for large n its covariance tends to the bound. In the present problem, this property holds for all but the first case (small number of measurements and marginal observability) from each group from Table I.

Fig. 9 shows the position error ellipses based on CRLB on the three target trajectories with heading 60°, 100° and 140°. The ellipses are drawn at time 10 s, 20 s, 30 s and 60 s, which correspond to batch sizes of $n = 10$, 20, 30 and 60, respectively. From the orientation of the ellipses, we can observe that main position error is along

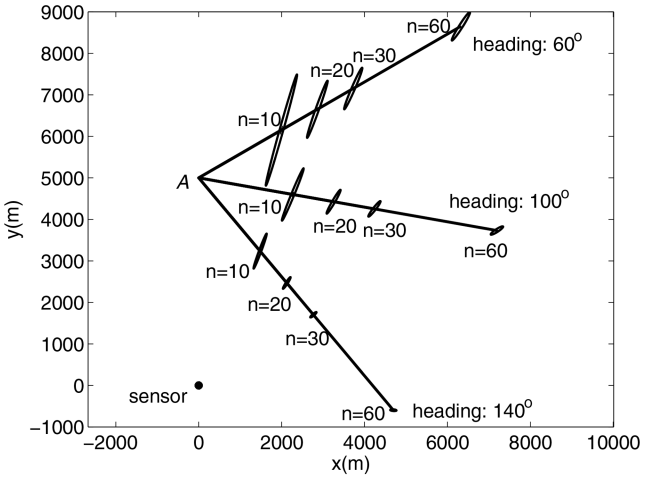

Fig. 9. Target position error ellipses based on CRLB. Three trajectories with heading 60°, 100° and 140° are shown. The position error ellipses are drawn for n = 10, 20, 30 and 60.

the bearing line, and the cross-bearing error is relatively small. This is reasonable and commonly occurs in the BOT estimation problem.

V. RECURSIVE STATE ESTIMATION

A. The Fusion Architecture

The recursive state estimation updates the target state as measurements are received. It can be seen from Fig. 1 that out-of-sequence measurements (OOSM) occur due to the acoustic propagation delay.

The OOSM problem is also referred to as "negative-time measurement update" problem, namely, the state emission time, $t_j^{e_2}$, corresponding to the latest measurement at $t_k^{s_2}$ is earlier than the latest state updating time, $t_i^{e_1}$, namely $t_j^{e_2} < t_i^{e_1}$ The prediction step in the in-sequence estimation becomes a retrodiction for the OOSM. The OOSM problem has been extensively studied [5]. The simplest approach performs an approximate retrodiction by neglecting the process noise [5]. This approach is referred to as Algorithm C in [5]. Algorithms B1 and A1 were proposed to solve the one-step-lag OOSM by considering the process noise [9] [3], and they give an approximate and the exact solutions, respectively. They were further developed to the algorithms Bl1 and Al1 for solving the l-step-lag OOSM ($l > 1$) in a single step [4].

The existing OOSM algorithms mentioned above assume that retrodiction time is known. However, the retrodiction time is the acoustic signal emission time in our problem. This is unknown to the observer and depends on the state of the target according to the following propagation delay constraint

$$t_j^{e_2} = t_k^{s_2} - \delta_{j,k} \tag{44}$$

where

$$\delta_{j,k} = \frac{r_{j,k}}{c^{\mathrm{p}}} \tag{45}$$

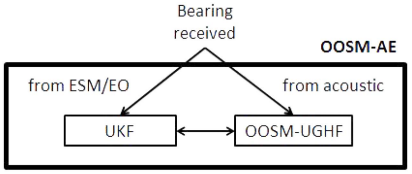

Fig. 10. OOSE-AE fusion architecture

is the propagation delay, c^{p} is the signal propagation speed in the medium, and $r_{j,k}$, which depends on the state (at the emission time), is the distance from the target at time $t_j^{e_2}$ to the sensor at time $t_k^{s_2}$. This leads to an implicit constraint in the state transition model.

Recently, we have formulated an implicit-constraint dynamic estimation problem using a Gauss-Helmert model (GHM), and presented an unscented Gauss-Helmert filter (UGHF) [23] [24] to solve this problem. The UGHF works only with in-sequence measurements. The development for the OOSM-UGHF is one of the main contributions of this paper.

The recursive estimation problem in this paper is to estimate the target state with fusion of in-sequence bearings from the ESM/EO sensor (s_1) and out-of-sequence bearings from the acoustic sensor (s_2). The algorithm is called out-of-sequence measurement fusion for acoustic and ESM/EO sensors (OOSM-AE). Its architecture is shown in Fig. 10. State estimation for the bearings from s_1 will be performed by a unscented Kalman filter (UKF), which will be given next. For s_2, a new OOSM-UGHF will be developed and described in Section VI.

B. The Model for the Recursive Estimation with Non-Delayed Bearings

The state estimation using the ESM/EO bearings is straightforward as the measurements arrive in-sequence and no propagation delay needs to be taken into consideration. The problem is formulated based on the nearly CV state model (or WNA—white noise acceleration). The target state, with dimension 4, is defined as

$$\mathbf{x}^4(t_k^{s_1}) = [x(t_k^{s_1})\ \ y(t_k^{s_1})\ \ \dot{x}(t_k^{s_1})\ \ \dot{y}(t_k^{s_1})]' \tag{46}$$

where $t_k^{s_1}$ is the signal reception (or sensor) time by the ESM/EO sensor s_1 at time cycle k. Since the propagation delay is negligible for s_1, the target signal emission time $t_i^{e_1}$ is equal to $t_k^{s_1}$. The state transition model is[3]

$$\mathbf{x}^4(t_k^{s_1}) = \mathbf{F}(t_k^{s_1}, t_{k-1}^{s_1})\mathbf{x}^4(t_{k-1}^{s_1}) + \mathbf{v}^4(t_k^{s_1}, t_{k-1}^{s_1}) \tag{47}$$

where the transition matrix is

$$\mathbf{F}(t_k^{s_1}, t_{k-1}^{s_1}) = \begin{bmatrix} 1 & 0 & T_{k,k-1} & 0 \\ 0 & 1 & 0 & T_{k,k-1} \\ 0 & 0 & 1 & 0 \\ 0 & 0 & 0 & 1 \end{bmatrix} \tag{48}$$

[3]Here it is assumed for simplicity that the measurements arriving at t_{k-1} and t_k are both from sensor s_1.

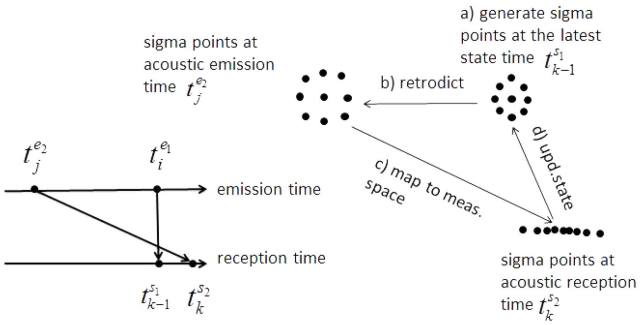

Fig. 11. OOSM-UGHF

and

$$T_{k,k-1} = t_k^{s_1} - t_{k-1}^{s_1} \tag{49}$$

with $\mathbf{v}^4$ the zero-mean process noise[4] (WNA) for the interval $(t_{k-1}^{s_1}, t_k^{s_1}]$. The discretized white noise acceleration (DWNA) model [2] has covariance

$$E[\mathbf{v}^4(\cdot)\mathbf{v}^4(\cdot)'] = \mathbf{Q}^4(t_k^{s_1}, t_{k-1}^{s_1}) = \begin{bmatrix} \frac{T_{k,k-1}^3}{3} & 0 & \frac{T_{k,k-1}^2}{2} & 0 \\ 0 & \frac{T_{k,k-1}^3}{3} & 0 & \frac{T_{k,k-1}^2}{2} \\ \frac{T_{k,k-1}^2}{2} & 0 & T_{k,k-1} & 0 \\ 0 & \frac{T_{k,k-1}^2}{2} & 0 & T_{k,k-1} \end{bmatrix} q \tag{50}$$

where q is the power spectral density (PSD) of the (acceleration) process noise (same for x and y, and assumed independent between the coordinates). The measurement model is given by

$$z(t_k^{s_1}) = h^4[\mathbf{x}^4(t_k^{s_1})] = \tan^{-1}\left[\frac{x(t_k^{s_1}) - x^s(t_k^{s_1})}{y(t_k^{s_1}) - y^s(t_k^{s_1})}\right] + w(t_k^{s_1}) \tag{51}$$

where $x^s(t_k^{s_1})$ and $y^s(t_k^{s_1})$ are the sensor positions at time $t_k^{s_1}$ in the x and y coordinates respectively, $w(t_k^{s_1})$ is zero-mean white Gaussian measurement noise with variance $R(t_k^{s_1})$, assumed independent of the process noise.

The unscented Kalman filter (UKF) is used to estimate the state as in [15].

VI. RECURSIVE STATE ESTIMATION WITH DELAYED BEARINGS

An out-of-sequence-measurement filter is required for the bearings from the acoustic sensor s_2. It can be seen in Fig. 11 that an acoustic measurement received at time $t_k^{s_2}$ corresponds to the target state at emission time $t_j^{e_2}$, which is earlier than the latest state assumed to have been updated by the ESM/EO sensor at time $t_{k-1}^{s_1} = t_i^{e_1}$. The problem is then to update the state estimate $\hat{\mathbf{x}}^4(t_{k-1}^{s_1} \mid t_{k-1}^{s_1})$ with the acoustic measurement $z(t_k^{s_2})$. The main challenge of this problem compared to the existing OOSM approaches is that the time $t_j^{e_2}$ is unknown, and it needs to be estimated together with the kinematic state.

Instead of the first-order Taylor linearization used in the existing OOSM algorithms [4] [5], the unscented transform is used in the above above mentioned problem. This consists of the following steps:

- Retrodict the state from time $t_i^{e_1} = t_{k-1}^{s_1}$ to the (unknown) emission time $t_j^{e_2}$ (to be estimated) corresponding to the sensor time $t_k^{s_2}$. The state estimate before retrodiction is $\hat{\mathbf{x}}^4(t_{k-1}^{s_1} \mid t_{k-1}^{s_1})$, and the retrodicted state is $\hat{\mathbf{x}}^5(t_j^{e_2} \mid t_{k-1}^{s_1})$. The latter, defined below in (52), includes the acoustic emission time. This step is illustrated through a) and b) in Fig. 11.
- Update the state estimate $\hat{\mathbf{x}}^4(t_{k-1}^{s_1} \mid t_{k-1}^{s_1})$ to $\hat{\mathbf{x}}^4(t_{k-1}^{s_1} \mid t_k^{s_2})$ with the acoustic OOSM $z(t_k^{s_2})$. This step is illustrated through c) and d) in Fig. 11.

The algorithm details are presented next.

A. State Retrodiction

The retrodiction that has to be done to the emission time $t_j^{e_2}$ (unknown to the observer) is subject to the propagation delay constraint described in (44). To estimate the retrodicted target kinematic information and the emission time $t_j^{e_2}$ simultaneously, the following augmented state is defined:

$$\mathbf{x}^5(t_j^{e_2}) = [x(t_j^{e_2}) \;\; y(t_j^{e_2}) \;\; \dot{x}(t_j^{e_2}) \;\; \dot{y}(t_j^{e_2}) \;\; t_j^{e_2}]' \tag{52}$$

Obviously, the positions $x(t_j^{e_2})$, $y(t_j^{e_2})$ and the time $t_j^{e_2}$ depend on each other, and this leads to the retrodicted state $\hat{\mathbf{x}}^5(t_j^{e_2} \mid t_{k-1}^{s_1})$ and the latest state estimate $\hat{\mathbf{x}}^4(t_{k-1}^{s_1} \mid t_{k-1}^{s_1})$ to have an implicit relationship. The Gauss-Helmert transition model [23] [24], which handles such implicit relationships, is then used for retrodiction. This is described by

$$\mathbf{g}[\mathbf{x}^5(t_j^{e_2}), \mathbf{x}^4(t_{k-1}^{s_1})] + \mathbf{v}^5(t_{k-1}^{s_1}, t_j^{e_2}) = \mathbf{0}_5 \tag{53}$$

where $\mathbf{g}[\cdot]$ is the Gauss-Helmert implicit state transition function, which combines the target motion constraints and the delay constraint between $\mathbf{x}^5(t_j^{e_2})$ of dimension 5 and $\mathbf{x}^4(t_{k-1}^{s_1})$ of dimension 4, and $\mathbf{0}_5$ is the zero vector of dimension 5. Assuming the target motion follows a WNA motion, $\mathbf{g}[\cdot]$ is given by

$$\mathbf{g}[\cdot] = [g_1(\cdot) \;\; g_2(\cdot) \;\; g_3(\cdot) \;\; g_4(\cdot) \;\; g_5(\cdot)]' \tag{54}$$

where

$$g_1 = x(t_j^{e_2}) - x(t_{k-1}^{s_1}) - \dot{x}(t_{k-1}^{s_1}) T_{j,k-1} \tag{55}$$

$$g_2 = y(t_j^{e_2}) - y(t_{k-1}^{s_1}) - \dot{y}(t_{k-1}^{s_1}) T_{j,k-1} \tag{56}$$

$$g_3 = \dot{x}(t_j^{e_2}) - \dot{x}(t_{k-1}^{s_1}) \tag{57}$$

$$g_4 = \dot{y}(t_j^{e_2}) - \dot{y}(t_{k-1}^{s_1}) \tag{58}$$

$$g_5 = t_j^{e_2} + \frac{r_{j,k}}{c^{\mathrm{p}}} - t_k^{s_2} \tag{59}$$

and

$$T_{j,k-1} = t_j^{e_2} - t_{k-1}^{s_1} < 0 \tag{60}$$

[4]The process noise arguments are shown in the same manner as for the state transition matrix.

$$r_{j,k} = \sqrt{[x(t_j^{e_2}) - x^s(t_k^{s_2})]^2 + [y(t_j^{e_2}) - y^s(t_k^{s_2})]^2} \quad (61)$$

Note that (59) is the equation that connects the emission time and target location to the corresponding sensor reception time.

The process noise $\mathbf{v}$[5] in (53) is modeled as zero-mean Gaussian. Based on the DWNA model [5], its covariance is

$$\mathbf{Q}^5(t_j^{e_2}, t_{k-1}^{s_1}) = \begin{bmatrix} \frac{|T_{j,k-1}|^3}{3}q & 0 & \frac{T_{j,k-1}^2}{2}q & 0 & 0 \\ 0 & \frac{|T_{j,k-1}|^3}{3}q & 0 & \frac{T_{j,k-1}^2}{2}q & 0 \\ \frac{T_{j,k-1}^2}{2}q & 0 & |T_{j,k-1}|q & 0 & 0 \\ 0 & \frac{T_{j,k-1}^2}{2}q & 0 & |T_{j,k-1}|q & 0 \\ 0 & 0 & 0 & 0 & q_\delta \end{bmatrix} \quad (62)$$

where q is as in (50), and q_δ is the variance of the process noise in the delay.

The algorithm used for retrodiction is the UGHF [24] [23], which obtains the retrodicted state iteratively through a Gauss-Newton algorithm. Given $\hat{\mathbf{x}}^4(t_{k-1}^{s_1} \mid t_{k-1}^{s_1})$ and its error covariance $\mathbf{P}^4(t_{k-1}^{s_1} \mid t_{k-1}^{s_1})$, the sigma points and their corresponding weights are

$$\{\{\hat{\mathbf{x}}^{4,m}(t_{k-1}^{s_1} \mid t_{k-1}^{s_1})\}, \{w^m\}\} = \text{SigmaPts}[\hat{\mathbf{x}}^4(t_{k-1}^{s_1} \mid t_{k-1}^{s_1}), \mathbf{P}^4(t_{k-1}^{s_1} \mid t_{k-1}^{s_1}), \kappa] \quad (63)$$

with[5]

$$\hat{\mathbf{x}}^{4,0}(t_{k-1}^{s_1} \mid t_{k-1}^{s_1}) = \hat{\mathbf{x}}^4(t_{k-1}^{s_1} \mid t_{k-1}^{s_1}) \quad (64)$$

$$\hat{\mathbf{x}}^{4,m}(t_{k-1}^{s_1} \mid t_{k-1}^{s_1}) = \hat{\mathbf{x}}^4(t_{k-1}^{s_1} \mid t_{k-1}^{s_1}) + \left[\sqrt{(4+\kappa)\mathbf{P}^4(t_{k-1}^{s_1} \mid t_{k-1}^{s_1})}\right]_{|m|} \quad (65)$$

$$m = 1, \ldots, 4 \quad (66)$$

$$\hat{\mathbf{x}}^{4,m}(t_{k-1}^{s_1} \mid t_{k-1}^{s_1}) = \hat{\mathbf{x}}^4(t_{k-1}^{s_1} \mid t_{k-1}^{s_1}) - \left[\sqrt{(4+\kappa)\mathbf{P}^4(t_{k-1}^{s_1} \mid t_{k-1}^{s_1})}\right]_{|m|}$$

$$m = -4, \ldots, -1$$

$$w^0 = \frac{\kappa}{4+\kappa} \quad (67)$$

$$w^m = \frac{1}{2(4+\kappa)} \quad |m| = 1, \ldots, 4 \quad (68)$$

where $m = -4, \ldots, 4$, is the sigma point index, $\left[\sqrt{(4+\kappa)\mathbf{P}^4(t_{k-1}^{e} \mid t_{k-1}^{s_1})}\right]_{|m|}$ indicates the $|m|$th column of the matrix $\left[\sqrt{(4+\kappa)\mathbf{P}^4(t_{k-1}^{s_1} \mid t_{k-1}^{s_1})}\right]$, and κ is a scalar that determines the spread of sigma points. Each sigma point is retrodicted from the previous target time $t_{k-1}^{s_1}$ to an unknown time $(t_j^{e_2})^m$. The problem is then to solve

$$\mathbf{g}[\hat{\mathbf{x}}^{5,m}(t_j^{e_2} \mid t_{k-1}^{s_1}), \hat{\mathbf{x}}^{4,m}(t_{k-1}^{s_1} \mid t_{k-1}^{s_1})] = \mathbf{0}_5 \quad m = -4, \ldots, 4 \quad (69)$$

Note that the process noise is not taken into consideration in the OOSM algorithm C.

The Gauss-Newton algorithm is applied to obtain the points $\hat{\mathbf{x}}^{5,m}(t_j^{e_2} \mid t_{k-1}^{s_1})$ iteratively. The iteration procedure (with index n) for the mth sigma point is

$$[\hat{\mathbf{x}}^{5,m}(t_j^{e_2} \mid t_{k-1}^{s_1})]^n = [\hat{\mathbf{x}}^{5,m}(t_j^{e_2} \mid t_{k-1}^{s_1})]^{n-1} + \mathbf{A}^{-1}\mathbf{g}[[\hat{\mathbf{x}}^{5,m}(t_j^{e_2} \mid t_{k-1}^{s_1})]^{n-1}, \hat{\mathbf{x}}^{4,m}(t_{k-1}^{s_1} \mid t_{k-1}^{s_1})] \quad (70)$$

where $\mathbf{A}$ (without arguments, for conciseness) is the Jacobian matrix given by

$$\mathbf{A} = \frac{\partial \mathbf{g}[[\hat{\mathbf{x}}^{5,m}(t_j^{e_2} \mid t_{k-1}^{s_1})]^n, \hat{\mathbf{x}}^{4,m}(t_{k-1}^{s_1} \mid t_{k-1}^{s_1})]}{\partial [\hat{\mathbf{x}}^{5,m}(t_j^{e_2} \mid t_{k-1}^{s_1})]^n} = \begin{bmatrix} 1 & 0 & 0 & 0 & -\dot{x}^m(t_{k-1}^{s_1} \mid t_{k-1}^{s_1}) \\ 0 & 1 & 0 & 0 & -\dot{y}^m(t_{k-1}^{s_1} \mid t_{k-1}^{s_1}) \\ 0 & 0 & 1 & 0 & 0 \\ 0 & 0 & 0 & 1 & 0 \\ \frac{x_{j,k}^r}{r_{j,k}c^{\mathrm{p}}} & \frac{y_{j,k}^r}{r_{j,k}c^{\mathrm{p}}} & 0 & 0 & 1 \end{bmatrix} \quad (71)$$

and

$$x_{j,k}^r \triangleq [x^m(t_j^{e_2} \mid t_{k-1}^{s_1})]^n - x^s(t_k^{s_2}) \quad (72)$$

$$y_{j,k}^r \triangleq [y^m(t_j^{e_2} \mid t_{k-1}^{s_1})]^n - y^s(t_k^{s_2}) \quad (73)$$

$$r_{j,k} \triangleq \sqrt{(x_{j,k}^r)^2 + (y_{j,k}^r)^2} \quad (74)$$

The Gauss-Newton algorithm described in (70) is quadratically convergent to the unique solution when a target is not approaching the sensor with radial speed c^{p}, if we assume the initial point is reasonably close to the solution [24].

The initial value of the mth sigma point $[\hat{\mathbf{x}}^{5,m}(t_j^{e_2} \mid t_{k-1}^{s_1})]^0$ for the iteration (70) is computed as

$$[x^m(t_j^{e_2} \mid t_{k-1}^{s_1})]^0 = x^m(t_{k-1}^{s_1} \mid t_{k-1}^{s_1}) + \dot{x}^m(t_{k-1}^{s_1} \mid t_{k-1}^{s_1})[\Delta(t_j^{e_2})]^0 \quad (75)$$

$$[y^m(t_j^{e_2} \mid t_{k-1}^{s_1})]^0 = y^m(t_{k-1}^{s_1} \mid t_{k-1}^{s_1}) + \dot{y}^m(t_{k-1}^{s_1} \mid t_{k-1}^{s_1})[\Delta(t_j^{e_2})]^0 \quad (76)$$

$$[\dot{x}^m(t_j^{e_2} \mid t_{k-1}^{s_1})]^0 = \dot{x}^m(t_{k-1}^{s_1} \mid t_{k-1}^{s_1}) \quad (77)$$

$$[\dot{y}^m(t_j^{e_2} \mid t_{k-1}^{s_1})]^0 = \dot{y}^m(t_{k-1}^{s_1} \mid t_{k-1}^{s_1}) \quad (78)$$

$$[(t_j^{e_2})^m]^0 = t_k^{s_2} - \delta_{j,k} \quad (79)$$

[5]Since $\hat{\mathbf{x}}^4(t_{k-1}^{s_1} \mid t_{k-1}^{s_1})$ has dimension 4, there are 9 sigma points [15].

where

$$[\Delta(t_j^{e_2})]^0 = [(t_j^{e_2})^m]^0 - t_{k-1}^{s_1} \tag{80}$$

$$\delta_{j,k} \approx r_{k-1}^m / c^{\mathrm{p}} \tag{81}$$

and r_{k-1}^m is the distance between the target position estimate and the sensor at time $t_{k-1}^{s_1}$.

The retrodicted state $\hat{\mathbf{x}}^5(t_j^{e_2} \mid t_{k-1}^{s_1})$ and its error covariance $\mathbf{P}^5(t_j^{e_2} \mid t_{k-1}^{s_1})$ are then computed from the following weighted sums of the retrodicted sigma points

$$\hat{\mathbf{x}}^5(t_j^{e_2} \mid t_{k-1}^{s_1}) = \sum_{m=-4}^{4} w^m \hat{\mathbf{x}}^{5,m}(t_j^{e_2} \mid t_{k-1}^{s_1}) \tag{82}$$

$$\mathbf{P}^5(t_j^{e_2} \mid t_{k-1}^{s_1}) \approx \sum_{m=-4}^{4} w^m \tilde{\mathbf{x}}^{5,m}(t_j^{e_2} \mid t_{k-1}^{s_1})(\tilde{\mathbf{x}}^{5,m}(t_j^{e_2} \mid t_{k-1}^{s_1}))' \tag{83}$$

where

$$\tilde{\mathbf{x}}^{5,m}(t_j^{e_2} \mid t_{k-1}^{s_1}) = \hat{\mathbf{x}}^{5,m}(t_j^{e_2} \mid t_{k-1}^{s_1}) - \hat{\mathbf{x}}^5(t_j^{e_2} \mid t_{k-1}^{s_1}) \tag{84}$$

with $m = -4, \ldots, 4$.

B. State Update

This step updates $\hat{\mathbf{x}}^4(t_{k-1}^{s_1} \mid t_{k-1}^{s_1})$ to $\hat{\mathbf{x}}^4(t_{k-1}^{s_1} \mid t_k^{s_2})$ by the OOSM $z(t_k^{s_2})$—it fuses the latter into the former. Note that the sigma points of $\hat{\mathbf{x}}^4(t_{k-1}^{s_1} \mid t_{k-1}^{s_1})$ have been generated in (63).

According to the linear minimum mean square error (LMMSE) estimator [2], the estimate $\hat{\mathbf{x}}^4(t_{k-1}^{s_1} \mid t_k^{s_2})$ and its error covariance $\mathbf{P}^4(t_{k-1}^{s_1} \mid t_k^{s_2})$ are given by

$$\hat{\mathbf{x}}^4(t_{k-1}^{s_1} \mid t_k^{s_2}) = \hat{\mathbf{x}}^4(t_{k-1}^{s_1} \mid t_{k-1}^{s_1}) + \mathbf{P}_{xz} P_{zz}^{-1}[z(t_k^{s_2}) - \hat{z}(t_k^{s_2})] \tag{85}$$

$$\mathbf{P}^4(t_{k-1}^{s_1} \mid t_k^{s_2}) = \mathbf{P}^4(t_{k-1}^{s_1} \mid t_{k-1}^{s_1}) - \mathbf{P}_{xz} P_{zz}^{-1} \mathbf{P}'_{xz} \tag{86}$$

The expected measurement $\hat{z}(t_k^{s_2})$, based on the retrodicted state $\hat{\mathbf{x}}^{5,m}(t_j^{e_2} \mid t_{k-1}^{s_1})$, is

$$\hat{z}(t_k^{s_2}) = \sum_{m=-4}^{4} w^m \hat{z}^m(t_k^{s_2}) \tag{87}$$

where

$$\begin{aligned} \hat{z}^m(t_k^{s_2}) &= h^5[\hat{\mathbf{x}}^{5,m}(t_j^{e_2} \mid t_{k-1}^{s_1})] \\ &= \tan^{-1}\left[\frac{x^m(t_j^{e_2} \mid t_{k-1}^{s_1}) - x^s(t_k^{s_2})}{y^m(t_j^{e_2} \mid t_{k-1}^{s_1}) - y^s(t_k^{s_2})}\right] \end{aligned} \tag{88}$$

The variance P_{zz} of the innovation and the covariance $\mathbf{P}_{xz}$ between the state to be estimated and the measurement are computed as

$$P_{zz} = \sum_{m=-4}^{4} w^m [\tilde{z}^m(t_k^{s_2})]^2 + R(t_k^{s_2}) \tag{89}$$

$$\mathbf{P}_{xz} = \sum_{m=-4}^{4} w^m \tilde{\mathbf{x}}^{4,m}(t_{k-1}^{s_1} \mid t_{k-1}^{s_1}) \tilde{z}^m(t_k^{s_2}) \tag{90}$$

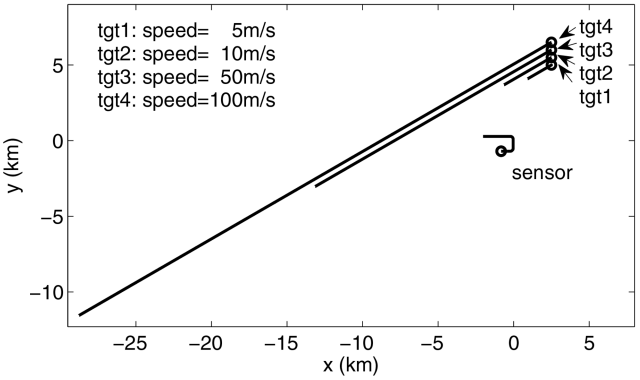

Fig. 12. Test scenarios. Initial locations of the targets and the maneuvering sensor platform are shown as "o." The stationary platform is located at (0,0)

where

$$\tilde{\mathbf{x}}^{4,m}(t_{k-1}^{s_1} \mid t_{k-1}^{s_1}) = \hat{\mathbf{x}}^{4,m}(t_{k-1}^{s_1} \mid t_{k-1}^{s_1}) - \hat{\mathbf{x}}^4(t_{k-1}^{s_1} \mid t_{k-1}^{s_1}) \tag{91}$$

$$\tilde{z}^m(t_k^{s_2}) = \hat{z}^m(t_k^{s_2}) - \hat{z}(t_k^{s_2}) \tag{92}$$

The OOSM-UGHF does not create new states, it only updates the state generated by the bearing from s_1 before.

VII. SIMULATION RESULTS FOR RECURSIVE ESTIMATION

Simulation results are given to demonstrate the new algorithm's performance. The conventional BOT approach is also evaluated using the same simulation data. Two sensor platform scenarios are used in the simulation tests:

- **Maneuvering (M)**: It has three legs linked by two 90° turns with turn rate 3°/s shown in Fig. 12. The platform speed is 10 m/s throughout the whole path. It moves to the east for 60 s, spends 30 s to make a 90° left turn, and moves to the north for 60 s. It then makes a 90° left turn, and moves towards the west for 180 s. The total duration is 360 s.
- **Stationary (S)**: The platform stays at position (0 m, 0 m) for 360 s.

An ESM sensor and an acoustic sensor are deployed on the platform to detect target bearings. The two sensors are not synchronized. Their sampling intervals and initial detection times are different. The ESM sensor is initiated at time 0 s with sampling interval 1s, whereas, the acoustic sensor is initiated at time 0.2 s with sampling interval 2 s. The 2:1 ratio of the sampling intervals is determined by the assumed reasonable sampling times of ESM and acoustic sensors. It can be set to other values based on real applications. The measured bearing errors of the ESM and the acoustic sensors are zero-mean white Gaussian with standard deviations $\sigma_b = 1°$. We assume that both sensors have no bearing detection during platform turns (total missed detection duration is

60 s for the maneuvering platform scenarios). This assumption is valid for most real applications. Typically, during a turn the pointing of the sensors is not known accurately.

Four targets moving at constant speeds of 5 m/s, 10 m/s, 50 m/s and 100 m/s, respectively, are shown in Fig. 12 (the actual trajectories have process noise, as discussed in the sequel). The state estimation starts 50 s after the targets move from their initial positions and the first bearing is from the ESM, so the acoustic signal can be guaranteed to reach the sensor platform when the estimation starts. This means that the targets are at their initial points at time −50 s, and the sensor platform is at its initial point at time 0 s. The estimation starts at time 0 s.

The algorithms used in the simulation are:

- **OOSM-AE**: The acoustic-ESM fusion algorithm proposed in this paper. The OOSM-UGHF is used for the bearings from the acoustic sensor, and the UKF is used for the bearings from the ESM. It works for both stationary and moving (maneuvering or nonmaneuvering) platform.
- **UKF-E**: A UKF to estimate state based on the ESM bearings only. The acoustic bearings are regarded as "expired" information and discarded. This algorithm is the conventional BOT approach, which works for maneuvering platform only.

The initial state estimate is

$$\hat{\mathbf{x}}^4(t_0^{s_1}) = [r_0 \sin b_0 \quad r_0 \cos b_0 \quad \dot{x}_0 \quad \dot{y}_0]' \tag{93}$$

where $b_0 = b(t_0^{s_1})$ is the ESM measured bearing at time $t_0^{s_1} = 0$ s,

$$r_0 \sim \mathcal{N}(\hat{r}_0, \sigma_{r_0}^2) \tag{94}$$

$$\dot{x}_0 \sim \mathcal{N}(0, \sigma_{\dot{x}_0}^2) \tag{95}$$

$$\dot{y}_0 \sim \mathcal{N}(0, \sigma_{\dot{y}_0}^2) \tag{96}$$

with $\hat{r}_0 = 7500$ m is half of the detection range (assuming 15000 m), $\sigma_{r_0} = 2500$ m, and $\sigma_{\dot{x}_0} = \sigma_{\dot{y}_0} = 30$ m/s. The initial state error covariance is computed by [20]

$$\mathbf{P}^4(t_0^{s_1}) = \begin{bmatrix} P_{xx} & P_{xy} & 0 & 0 \\ P_{yx} & P_{yy} & 0 & 0 \\ 0 & 0 & \sigma_{\dot{x}_0}^2 & 0 \\ 0 & 0 & 0 & \sigma_{\dot{y}_0}^2 \end{bmatrix} \tag{97}$$

where

$$P_{xx} = (\hat{r}_0 \sigma_b \cos b_0)^2 + (\sigma_r \sin b_0)^2 \tag{98}$$

$$P_{yy} = (\hat{r}_0 \sigma_b \sin b_0)^2 + (\sigma_r \cos b_0)^2 \tag{99}$$

$$P_{xy} = P_{yx} = (\sigma_r^2 - \hat{r}_0^2 \sigma_b^2) \sin b_0 \cos b_0 \tag{100}$$

In other words, in each run we have a random initial state, which is in accordance with the Bayesian model (see, e.g. [2] Sec. 5.5).

The process noise PSD q in (50) is set to $0.01\text{m}^2/\text{s}^3$. Note that due to the presence of process noise, batch estimation is not applicable. The acoustic signal propagation speed c^{p} in the air is 344 m/s. The scalar κ in (63)–(68) is set to 1.

The UGHF-E performance is investigated below in several aspects.

A. Root Mean Square Errors

The estimated position root mean square errors (RMSE) obtained from 100 Monte Carlo runs versus time are displayed in Figs. 13–16 for the maneuvering platform, and Figs. 17–18 for the stationary platform. The overall and the last point position RMSEs for all the scenarios are given in Table II. The RMSEs of the UKF-E are not shown in this table for the stationary platform, because the targets are unobservable in this case. The overall position RMSE for a particular scenario is computed by

$$\text{pos}^{\text{RMSE}} = \sqrt{\frac{1}{NK} \sum_{i=1}^{N} \sum_{k=1}^{K} [\text{pos}_i^{\text{err}}(t_k^{s_1})]^2} \tag{101}$$

where i is the run index, $N = 100$ is the number of runs, $K = 360$ is the number of time cycles in the scenario, and

$$\text{pos}^{\text{err}}(t_k^{s_1}) = \sqrt{[\hat{x}(t_k^{s_1}) - x(t_k^{s_1})]^2 + [\hat{y}(t_k^{s_1}) - y(t_k^{s_1})]^2} \tag{102}$$

where $\hat{x}(t_k^{s_1})$ and $\hat{y}(t_k^{s_1})$ are the estimated target positions, and $x(t_k^{s_1})$ and $y(t_k^{s_1})$ are the true target positions.

It can be seen that the OOSM-AE clearly outperforms the UKF-E for the maneuvering platform scenarios. The overall accuracy improvement in terms of position RMSE reduction is from 69% to 77%, a significant improvement. For the slow moving targets (shown in Figs. 13–14), the UKF-E takes a longer time to converge. The UKF-E position RMSEs start to decrease at time 180 s (after the second turn), whereas the RMSE reduction of the OOSM-AE occurs around time 50 s, which is much earlier than for the UKF-E. For the fast moving targets (shown in Figs. 15–16), both algorithms converge fast at the beginning, but the UKF-E has larger errors after a while.

For the stationary platform (Figs. 17–18), the OOSM-AE provides reliable estimation, whereas the UKF-E diverges since BOT from a single fixed passive sensor is not observable.

We also observe that the OOSM-AE has better performance for the fast moving targets than the slow moving targets in both maneuvering and stationary platform scenarios. The reason for this is that the slow moving targets have lower bearing change rate. The information provided by these slowly changing bearings is limited when they are "buried in the noise," and this results in marginal observability and slow convergence in the beginning. This effect is more serious for the stationary platform as its bearing change rate is even smaller than for the maneuvering platform.

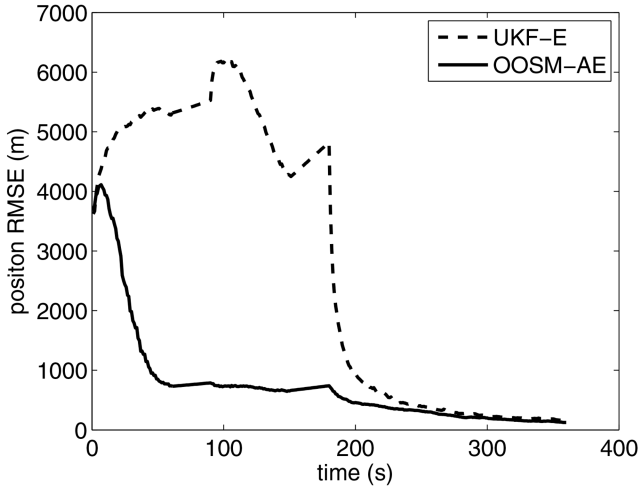

Fig. 13. Maneuvering platform: The estimated position RMSE versus time for the target with speed 5 m/s.

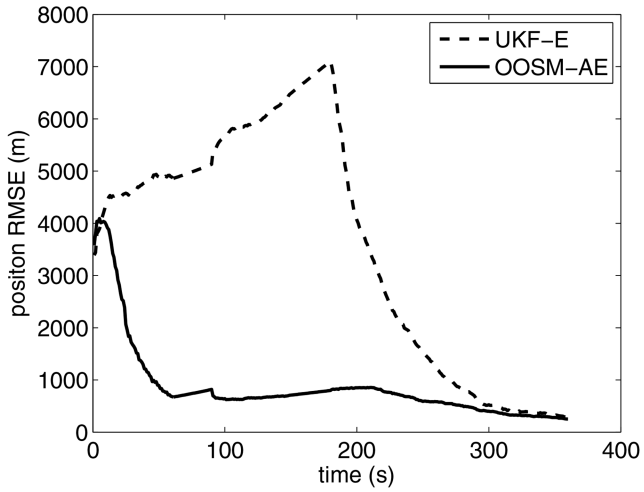

Fig. 14. Maneuvering platform: The estimated position RMSE versus time for the target with speed 10 m/s.

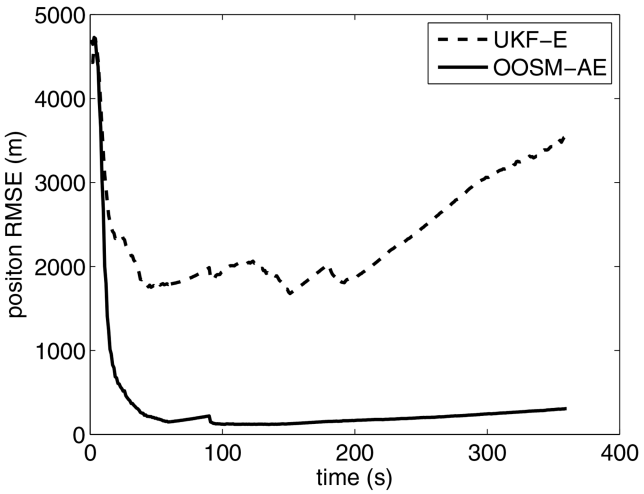

Fig. 15. Maneuvering platform: The estimated position RMSE versus time for the target with speed 50 m/s.

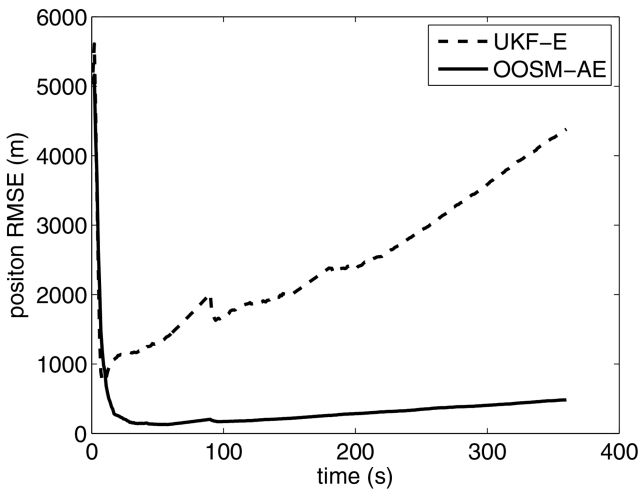

Fig. 16. Maneuvering platform: The estimated position RMSE versus time for the target with speed 100 m/s.

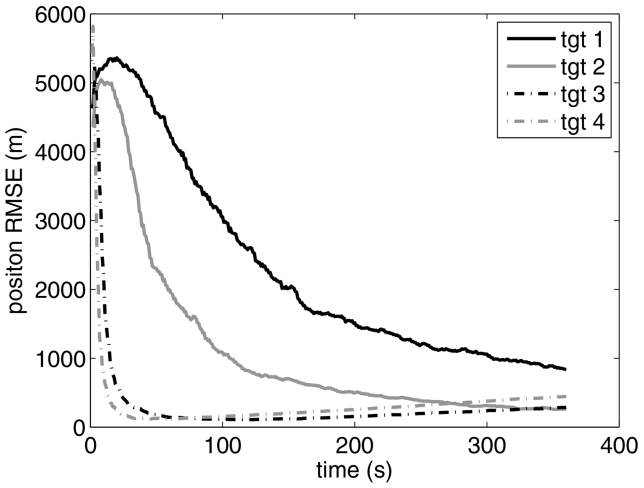

Fig. 17. Stationary platform: The OOSM-AE estimated position RMSE versus time for the targets with speeds of 5 m/s (tgt 1), 10 m/s (tgt 2), 50 m/s (tgt 3) and 100 m/s (tgt 4).

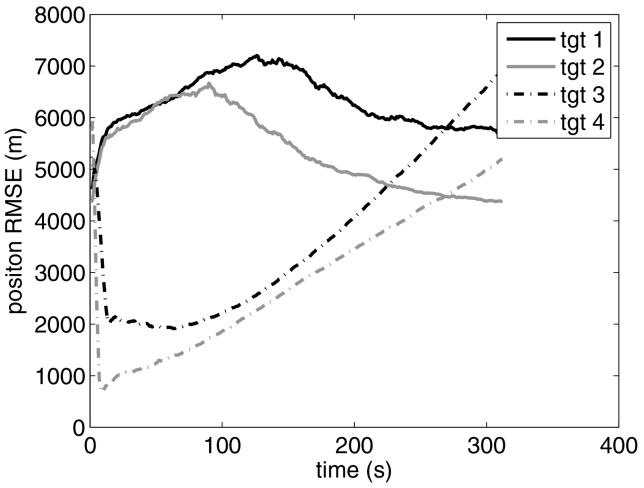

Fig. 18. Stationary platform: The UKF-E estimated position RMSE versus time for the four targets with speeds of 5 m/s (tgt 1), 10 m/s (tgt 2), 50 m/s (tgt 3) and 100 m/s (tgt 4).

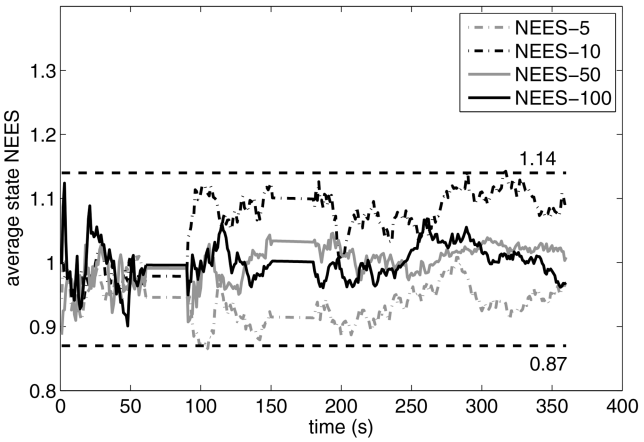

Fig. 19. The average state NEES (from 100 runs) for maneuvering platform scenarios with target speeds 5 m/s (NEES-5), 10 m/s (NEES-10), 50 m/s (NEES-50) and 100 m/s (NEES-100).

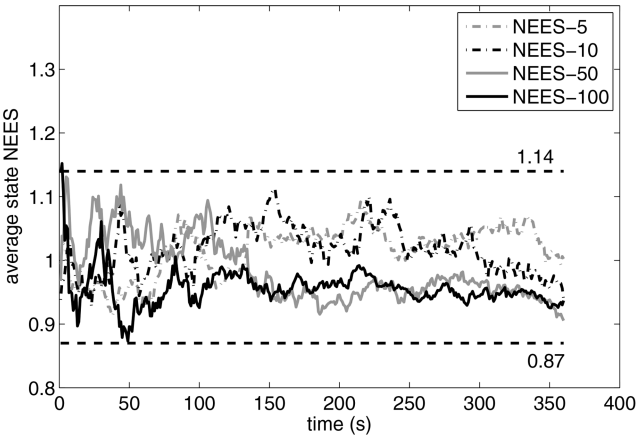

Fig. 20. The average state NEES (from 100 runs) for stationary platform scenarios with target speeds 5 m/s (NEES-5), 10 m/s (NEES-10), 50 m/s (NEES-50) and 100 m/s (NEES-100).

TABLE II
Position RMSEs for all the scenarios

		Overall RMSE			Last point RMSE	
Platform	Target speed (m/s)	OOSM-AE (m)	UKF-E (m)	Improvement (%)	OOSM-AE (m)	UKF-E (m)
M	5	1134.4	3694.5	69.3	124.2	156.3
	10	1152.4	4261.3	73.0	252.1	289.1
	50	752.5	2461.4	69.4	307.0	3540.7
	100	609.3	2673.5	77.2	483.9	4381.5
S	5	2724.2	—	—	836.2	—
	10	1708.2	—	—	261.3	—
	50	755.7	—	—	286.7	—
	100	624.2	—	—	445.0	—

B. Statistical Analysis: Consistency and Efficiency

To evaluate the consistency of OOSM-AE, the average normalized estimation error squared (NEES) is evaluated. The average state NEES at time t_k^s for N Monte Carlo runs is [2]

$$\bar{\epsilon}(t_k^s) = \frac{1}{n_{\mathbf{x}^4} N} \sum_{i=1}^{N} \tilde{\mathbf{x}}_i^4(t_k^s)' \mathbf{P}^{-1}(t_k^s) \tilde{\mathbf{x}}_i^4(t_k^s) \tag{103}$$

where $\mathbf{P}(t_k^s)$ is the state error covariance computed by the OOSM-AE estimator, $n_{\mathbf{x}^4} = 4$ is the state dimension, i is the run index, and

$$\tilde{\mathbf{x}}_i^4(t_k^s) = \mathbf{x}^4(t_k^s) - \hat{\mathbf{x}}_i^4(t_k^s) \tag{104}$$

The two-sided 95% probability region for a 400 degrees of freedom ($N = 100$, $n_{\mathbf{x}^4} = 4$) chi-square random variable is [346.5, 457.3]. Dividing by 400, the average NEES should be in the interval [0.87, 1.14]. Figs. 19 and 20 show the average NEES versus time in the OOSM-AE for the maneuvering and stationary platform, respectively, where n in NEES-n stands for the target speed. It can be seen that the NEES for all test cases are within the range. This shows that OOSM-AE yields consistent estimation results.

Please note that the initial state for each run is randomly generated based on (93) with

$$r_0 \sim \mathcal{N}(r_0^{\text{true}}, \sigma_{r_0}^2) \tag{105}$$

$$\dot{x}_0 \sim \mathcal{N}(\dot{x}_0^{\text{true}}, \sigma_{\dot{x}_0}^2) \tag{106}$$

$$\dot{y}_0 \sim \mathcal{N}(\dot{y}_0^{\text{true}}, \sigma_{\dot{y}_0}^2) \tag{107}$$

where r_0^{true}, $\dot{x}_0^{\text{true}}$ and $\dot{y}_0^{\text{true}}$ are true values at time 0, and the error standard deviations are

$$\sigma_{r_0} = 0.2 r_0^{\text{true}} \tag{108}$$

$$\sigma_{\dot{x}_0} = 0.2 \dot{x}_0^{\text{true}} \tag{109}$$

$$\sigma_{\dot{y}_0} = 0.2 \dot{y}_0^{\text{true}} \tag{110}$$

This setting prevents the initial state (randomly generated) from bias and apart from the ground truth significantly (which may cause divergency).

The efficiency of the OOSM-AE can be studied through the posterior CRLB (PCRLB) which is also called Bayesian CRLB (BCRLB). It is the inverse of the Bayesian information matrix (BIM), $\mathbf{J}$ [21]. An estimator with state error $\tilde{\mathbf{x}}_i^4(t_k^s)$ is statistically efficient iff

$$\frac{1}{n_{\mathbf{x}^4}} E[\tilde{\mathbf{x}}_i^4(t_k^s)' \mathbf{J}(t_k^s) \tilde{\mathbf{x}}_i^4(t_k^s)] = 1 \tag{111}$$

where $\mathbf{J}(t_k^s)$ is the BIM at time t_k^s. Since $\mathbf{P}^{-1}(t_k^s)$ is a good (run-specific) approximation of $\mathbf{J}(t_k^s)$[6] (the former is conditioned on the measurements, while the latter is the average over all the measurements and states), the NEES (from 100 runs) can than be used to evaluate the estimator efficiency. It can be seen the NEES in Figs. 19 and 20 are within the 95% probability region.

[6]Based on our best knowledge, the BIM for the UGHF has not studied in literature. $\mathbf{P}^{-1}(t_k^s)$ is therefore used as the approximation of BIM.

VIII. CONCLUSIONS

This paper presented a new passive BOT approach through fusion of an ESM/EO and an acoustic sensor deployed on the same sensor platform. The OOSM-AE algorithm has been developed to estimate the target trajectory by utilizing the acoustic propagation delay which contains target range information. This approach avoids the requirement for platform maneuvers of the conventional BOT. The observability study conducted for this problem showed that the target state is completely observable when its bearing from the sensor platform is not a constant over time. Two algorithms, the ML estimator computed via ILS and OOSM-AE, were developed for batch and recursive estimations, respectively. Simulation results showed that the OOSM-AE can estimate the target trajectory effectively even from a stationary platform, and provides significant accuracy improvement (69%–77%) over the conventional BOT for the maneuvering platform cases considered. Statistical studies on consistency and efficiency were also conducted. The ML estimates obtained via ILS for a constant velocity target are statistically efficient, except for the case with too few measurements and marginal observability. The OOSM-AE yields consistent estimation results, and its average NEES is close 1. Thus, the new approach has the potential to enhance passive BOT capability significantly.

REFERENCES

[1] Aidala, V. J.
Kalman filter behavior in bearings-only tracking applications,
IEEE Transactions on Aerospace and Electronic Systems, 15, 1 (Jan. 1979), 29–39.

[2] Bar-Shalom, Y., Li, X. R. and Kirubarajan, T.
Estimation with Applications to Tracking and Navigation: Theory, Algorithms and Software,
New York: Wiley, 2001.

[3] Bar-Shalom, Y.
Update with out-of-sequence measurements in tracking: Exact Solution,
IEEE Transactions on Aerospace and Electronic Systems, 38, 3 (Jul. 2002), 769–778.

[4] Bar-Shalom, Y., Chen, H. M., and Mallick, M.
One-Step Solution for the Multistep Out-of-Sequence Measurement Problem in Tracking,
IEEE Transactions on Aerospace and Electronic Systems, 40, 1 (Jan. 2004), 27–37.

[5] Bar-Shalom, Y., Willett, P. K. and Tian, X.
Tracking and Data Fusion: A Handbook of Algorithms,
YBS Publishing, 2011.

[6] Le Cadre, J. P. and Jauffret, C.
Discrete-time observability and estimability analysis for bearings-only target motion analysis,
IEEE Transactions on Aerospace and Electronic Systems, 33, 1 (Jan. 1997), 178–201.

[7] Clavard, J., Pillon, D., Pignol, A-C. and Jauffret, C.
Target motion analysis of a source in a constant turn from a nonmaneuvering observer,
IEEE Transactions on Aerospace and Electronic Systems, 49, 3 (Jul. 2013), 1760–1780.

[8] Deb, S., Yeddanapudi, M., Pattipati, K. R. and Bar-Shalom, Y.
A generalized S-D assignment algorithm for multisensor-multitarget state estimation,
IEEE Transactions on Aerospace and Electronic Systems, 33, 2 (Apr. 1997), 523–538.

[9] Hilton, R. D., Martin, D. A., and Blair, W. D.
"Tracking with time-delayed data in multisensor systems,"
NSWCDD/TR-93/351, Dahlgren, VA, Aug. 1993.

[10] Jauffret C. and Bar-Shalom, Y.
Track Formation with Bearing and Frequency Measurements in Clutter,
IEEE Transactions on Aerospace Electronic Systems, 26, 6 (Nov. 1990), 999–1009.

[11] Jauffret, C. and Pillon, D.
Observability in passive target motion analysis,
IEEE Transactions on Aerospace and Electronic Systems, 32, 4 (Oct.1996), 1290–1300.

[12] Jauffret, C.
Observability and Fisher information matrix in nonlinear regression,
IEEE Transactions on Aerospace and Electronic Systems, 43, 2 (Apr. 2007), 756–759.

[13] Jauffret, C., Pillon, D., and Pignol, A-C.
Bearings-only maneuvering target motion analysis from a nonmaneuvering platform,
IEEE Transactions on Aerospace and Electronic Systems, 46, 4 (Oct. 2010), 1934–1948.

[14] Jauffret, C. and Pignol, A-C.
Target motion analysis by inverse triangulation,
Proc. 18th International Conference on Information Fusion, Washington, DC, Jul. 2015.

[15] Julier, S. J., and Uhlmann, J. K.
A new extension of the Kalman filter to nonlinear systems,
Proceedings of AeroSense: The 11th International Symposium on Aerospace/Defence Sensing, Simulation and Controls, Apr. 1997.

[16] Lindgren, A. G., and Gong, K. F.
Position and velocity estimation via bearing observations,
IEEE Transactions on Aerospace and Electronic Systems, 14, 4 (Jul. 1978) 564–577.

[17] Nardone, S. C., and Aidala, V. J.
Observability criteria for bearings-only target motion analysis,
IEEE Transactions on Aerospace and Electronic Systems, 17, 2 (Mar. 1981), 162–166.

[18] Passerieux, J. M., Pillon, D., Blanc-Benon, P., and Jauffret, C.
Target Motion Analysis with Bearing and Frequencies Measurements,
Proceedings of the 22nd Asilomar Conference, Pacific Grove, CA, USA, Nov. 1988.

[19] Pattipati, K. R., Deb, S., and Bar-Shalom, Y.
A new relaxation algorithm and passive sensor data association,
IEEE Transactions on Automatic Control, 37, 2 (Feb. 1992), 198–213.

[20] Ristic, B., Arulampalam, S., and Gordon N.
Beyond the Kalman Filter: Particle Filters for Tracking Applications,
Boston London: Artech House, 2004.

[21] Tichavsky, P., Muravchik, C. H., and Nehorai A.
Posterior Cramer-Rao bounds for discrete-time nonlinear filtering,
IEEE Transations on Signal Process, 46, 5 (May 1998), 1386–1396.

[22] Yang, R., Bar-Shalom, Y., and Ng, G. W.
Tracking/fusion and deghosting with Doppler frequency from two passive acoustic sensor,
Proc. 16th International Conference on Information Fusion, Istanbul, Turkey, Jul. 2013.

[23] Yang, R., Bar-Shalom, Y., Huang, J. H., and Ng, G. W.
Interacting multiple model unscented Gauss-Helmert filter for bearings-only tracking with state-dependent propagation delay,
Proc. 17th International Conference on Information Fusion, Salamanca, Spain, Jul. 2014.

[24] Yang, R., Bar-Shalom, Y., Huang, J. H., and Ng, G. W.
UGHF for acoustic tracking with state-dependent propagation delay,
IEEE Transactions on Aerospace and Electronic Systems, 51, 3 (Jul. 2015), 1747–1761.

[25] Yang, R., Bar-Shalom, Y., and Ng, G. W.
Bearings-only tracking with fusion from heterogenous passive sensors: ESM/EO and acoustic,
Proc. 18th International Conference on Information Fusion, Washington, DC, Jul. 2015.

Rong Yang received her B.E. degree in information and control from Xi'an Jiao Tong University, China in 1986, M.Sc. degree in electrical engineering from the National University of Singapore in 2000, and Ph.D. degree in electrical engineering from Nanyang Technological University, Singapore in 2012. She is currently a Principal Member of Technical Staff at DSO National Laboratories, Singapore. Her research interests include passive tracking, low observable target tracking, GMTI tracking, hybrid dynamic estimation and data fusion. She received the FUSION 2014 Best Paper Award (First runner up).

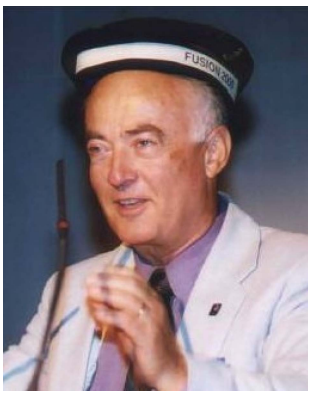

Yaakov Bar-Shalom was born on May 11, 1941. He received the B.S. and M.S. degrees from the Technion, Israel Institute of Technology, in 1963 and 1967 and the Ph.D. degree from Princeton University in 1970, all in electrical engineering. From 1970 to 1976 he was with Systems Control, Inc., Palo Alto, California. Currently he is Board of Trustees Distinguished Professor in the Dept. of Electrical and Computer Engineering and Marianne E. Klewin Professor in Engineering at the University of Connecticut. He is also Director of the ESP (Estimation and Signal Processing) Lab. His current research interests are in estimation theory, target tracking and data fusion. He has published over 500 papers and book chapters in these areas and in stochastic adaptive control. He coauthored the monograph Tracking and Data Association (Academic Press, 1988), the graduate texts Estimation and Tracking: Principles, Techniques and Software (Artech House, 1993; translated into Russian, MGTU Bauman, Moscow, Russia, 2011), Estimation with Applications to Tracking and Navigation: Algorithms and Software for Information Extraction (Wiley, 2001), the advanced graduate texts Multitarget-Multisensor Tracking: Principles and Techniques (YBS Publishing, 1995), Tracking and Data Fusion (YBS Publishing, 2011), and edited the books Multitarget-Multisensor Tracking: Applications and Advances (Artech House, Vol. I, 1990; Vol. II, 1992; Vol. III, 2000). He has been elected Fellow of IEEE for "contributions to the theory of stochastic systems and of multi-target tracking." He has been consulting to numerous companies and government agencies, and originated the series of Multitarget-Multisensor Tracking short courses offered via UCLA Extension, at Government Laboratories, private companies and overseas. During 1976 and 1977 he served as Associate Editor of the IEEE Transactions on Automatic Control and from 1978 to 1981 as Associate Editor of Automatica. He was Program Chairman of the 1982 American Control Conference, General Chairman of the 1985 ACC, and Co-Chairman of the 1989 IEEE International Conference on Control and Applications. During 1983–87 he served as Chairman of the Conference Activities Board of the IEEE Control Systems Society and during 1987–89 was a member of the Board of Governors of the IEEE CSS. He was a member of the Board of Directors of the International Society of Information Fusion (1999–2004) and served as General Chairman of FUSION 2000, President of ISIF in 2000 and 2002 and Vice President for Publications in 2004–13. In 1987 he received the IEEE CSS Distinguished Member Award. Since 1995 he is a Distinguished Lecturer of the IEEE AESS and has given numerous keynote addresses at major national and international conferences. He is co-recipient of the M. Barry Carlton Award for the best paper in the IEEE Transactions on Aerospace and Electronic Systems in 1995 and 2000 and recipient of the 1998 University of Connecticut AAUP Excellence Award for Research. In 2002 he received the J. Mignona Data Fusion Award from the DoD JDL Data Fusion Group. He is a member of the Connecticut Academy of Science and Engineering. In 2008 he was awarded the IEEE Dennis J. Picard Medal for Radar Technologies and Applications, and in 2012 the Connecticut Medal of Technology. In 2015, he received from the International Society for Information Fusion the Lifetime of Excellence in Information Fusion award. He has been listed by academic.research.microsoft (top authors in engineering) as #1 among the researchers in Aerospace Engineering based on the citations of his work.

Gee Wah Ng received his M.Sc. and Ph.D. from University of Manchester Institute of Science and Technology, United Kingdom. He is currently a Distinguished Member of Technical Staff and Programme Director (Information Exploitation) of Information Division at DSO National Laboratories. He has delivered many projects in the decision support areas and has authored three books. He is active in international conferences in the areas of information fusion and intelligent systems. His research interests in data and information fusion include target tracking, computational intelligence, machine learning, self-tuning and sensor networks.